

WHY OPTICALLY-FAINT AGN ARE OPTICALLY-FAINT: THE *Spitzer* PERSPECTIVE

J. R. RIGBY¹, G. H. RIEKE¹, P. G. PÉREZ-GONZÁLEZ¹, J. L. DONLEY¹, A. ALONSO-HERRERO^{1,2}, J.-S. HUANG³,
 P. BARMBY³, & G. G. FAZIO³

Accepted for publication in the Astrophysical Journal

ABSTRACT

Optically-faint X-ray sources (those with $f_X/f_R > 10$) constitute about 20% of X-ray sources in deep surveys, and are potentially highly obscured and/or at high redshift. Their faint optical fluxes are generally beyond the reach of spectroscopy. For a sample of 20 optically-faint sources in CDFS, we compile 0.4–24 μm photometry, relying heavily on *Spitzer*. We estimate photometric redshifts for 17 of these 20 sources. We find that these AGN are optically-faint both because they lie at significantly higher redshifts (median $z \sim 1.6$) than most X-ray-selected AGN, and because their spectra are much redder than standard AGN. They have 2–8 keV X-ray luminosities in the Seyfert range, unlike the QSO-luminosities of optically-faint AGN found in shallow, wide-field surveys. Their contribution to the X-ray Seyfert luminosity function is comparable to that of $z > 1$ optically-bright AGN.

Subject headings: galaxies: active—X-rays: galaxies—infrared: galaxies

1. INTRODUCTION

Deep X-ray surveys have resolved the X-ray background into discrete sources, verifying that it is the combined output of obscured and unobscured active galactic nuclei (AGN) (e.g., Moretti et al. 2003). The challenge now is to establish the redshift, luminosity, and column density distributions of these AGN, and the properties of their host galaxies, to understand AGN evolution and accretion history. About 35% of the X-ray detections in 1 Ms observations are beyond the reach of spectroscopy. They are expected to be more heavily obscured and/or at higher redshift than the brighter population. A subset of these X-ray sources are much dimmer in the optical, relative to their X-ray fluxes, than ordinary AGN, and have thus been termed the “optically-faint AGN.” They are interesting in two ways.

First, they are likely to be highly obscured: they lack the bright blue continua so prominent in unobscured AGN, and their X-ray photon indices indicate more obscuration than in Type 1 AGN. Obscured AGN are expected to dominate the faint number counts and the power in the background above a few keV.

Second, these optically-faint AGN may lie at high redshift. Pre-*Chandra* X-ray background models predicted an AGN redshift distribution that peaked at $z = 1.3$ – 1.5 (Gilli et al. 1999, 2001). By contrast, the redshift distribution of *Chandra*-selected AGN found by spectroscopic follow-up is much lower, peaking near $z \sim 0.7$ (Gilli 2003). Models using a post-*Chandra* luminosity function (LF) can accommodate a lower-redshift distribution (Ueda et al. 2003), but an alternative possibility is that the distribution does peak at higher redshift, but significant numbers of high-redshift AGN have been systematically excluded from the spectroscopic surveys.

The general properties of optically-faint AGN and

similar objects have been studied by Alexander et al. (2001), Yan et al. (2003), and Koekemoer et al. (2004), but without redshift estimation. Zheng et al. (2004) used optical and near-infrared photometry to obtain photometric redshifts for 99% of the X-ray-selected AGN in the CDFS, including most of the optically-faint objects. However, such redshifts are extremely difficult to obtain for optically-faint sources, and of unproven reliability. We combine optical, near-infrared, and most importantly, mid-infrared (from *Spitzer*) photometry to obtain independent redshifts. *Spitzer* is ideally suited to find redshifts for these sources: the IRAC bands (at 3.6, 4.5, 5.8, and 8.0 μm) are well-placed to sample the stellar emission of even very high redshift galaxies. Additionally, the rest-frame near infrared (which *Spitzer* probes for $z \geq 1$) typically offers the highest contrast to detect the normal stellar population against the AGN light. Thus, the IRAC bands have the best chance of revealing stellar features that can yield redshift determinations.

2. THE X-RAY-TO-OPTICAL FLUX RATIO AND SAMPLE SELECTION

The ratio of optical R-band flux to hard X-ray (usually 2–10 keV or 2–8 keV) flux, (f_X/f_R), can be used to classify the emission mechanisms of X-ray sources (e.g. Maccacaro et al. 1988; Comastri et al. 2002; Barger et al. 2003). A value < 0.01 indicates the X-ray emission is powered by star formation, while $0.1 < f_X/f_R < 10$ indicates that the X-rays arise in an AGN. Optically-faint X-ray sources are defined to have $f_X/f_R > 10$, making them poor emitters at optical wavelengths given their X-ray fluxes. The f_X/f_R ratio is defined in the observed frame, and as such is subject to K-corrections.

In this paper, we use the f_X/f_R ratio to select optically-faint AGN. The region sampled is the overlap between the *Chandra* Deep Field South 1 Ms *Chandra* observation (Giacconi et al. 2002; Alexander et al. 2003) and the GOODS ACS optical mosaic (Giavalisco et al. 2004). We start by choosing objects from the Giacconi et al. (2002) X-ray catalog that have 2–10 keV band detections and $f_X/f_R > 10$. When Giacconi et al. (2002) list multiple R-band candidate counterparts for an X-ray source, we

¹ Steward Observatory, University of Arizona, 933 N. Cherry Ave., Tucson, AZ 85721

² Instituto de Estructura de la Materia, Consejo Superior de Investigaciones Científicas, E-28006 Madrid, Spain

³ Harvard-Smithsonian Center for Astrophysics, 60 Garden Street, Cambridge, MA, 02138

require they all be optically-faint. If no R-band counterpart is detected, we require a flux upper limit stringent enough to insure $f_X/f_R > 10$. These criteria select 48 sources.

We then switch to the Alexander et al. (2003) CDFS X-ray catalog, since it has smaller R-to-X-ray positional offsets than does Giacconi et al. (2002) catalog (see the appendix of Alexander et al. 2003.) We do this by cross-correlating the two X-ray catalogs, requiring hard-band detection in both catalogs within $1.6''$. This drops 9 sources from the sample: 3 of the sources have no counterpart in the Alexander et al. (2003) catalog, even out to $5''$; and 6 are 2–8 keV non-detections (but are detected in another band) in the Alexander et al. (2003) catalog, and thus are dropped from our sample. The 9 dropped sources are fainter than the optically-faint sample, with 2–8 keV fluxes $\lesssim 10^{-15}$ erg s $^{-1}$ cm $^{-2}$, as compared to the median 2–8 keV flux for the 39 optically-faint sources of 3.6×10^{-15} erg s $^{-1}$ cm $^{-2}$.

All but 6 of the 39 optically-faint sources have 2–8 keV and 0.5–2 keV fluxes that agree within 20% between both X-ray catalogs.⁴ Sources are identified by ID numbers from Alexander et al. (2003) (abbreviated AID).

To obtain a sample with high-quality SEDs, we then a) choose those sources that lie within the GOODS ACS field, which reduces the sample to 25; and b) require each source to have at least two photometric detections at wavelengths below $1 \mu\text{m}$, which further reduces the sample to 20 AGN. We term the resulting sample of 20 AGN the “complete-SED sample (CSS)”.

There are two potential sources of biases to this sample. First, it may be somewhat brighter than the remaining optically-faint AGN, due to the requirement for multiple-band optical detections. Second, requiring $\lambda < 1 \mu\text{m}$ detections might possibly bias the CSS toward low redshifts compared to the full sample of optically-faint AGN; we explore this possibility in § 5, by examining the redshifts of sources that would be excluded by the $\lambda < 1 \mu\text{m}$ detection requirement.

3. *Spitzer* OBSERVATIONS, PHOTOMETRY, AND SEDS

With *Spitzer* (Werner et al. 2004), we obtained IRAC (Fazio et al. 2004) measurements of the CDFS with 500 s of integration. The images were reduced by the *Spitzer* Science Center using the standard pipeline. We also obtained MIPS (Rieke et al. 2004) $24 \mu\text{m}$ scan map images with a total integration time of ~ 1200 s per position, nominally composed of 120 individual sightings per source. These data were reduced using the instrument team data analysis tool (Gordon et al. 2005), creating the image presented by Rigby et al. (2004).

We created a database to combine the MIPS and IRAC images with the following optical and near-infrared imagery: the ACS/HST *bviz* images from GOODS (Giavalisco et al. 2004); *RIz* frames from the Las Campanas Infrared Survey (Marzke et al. 1999); and the *BVRI* images released by the ESO Imaging Survey (Arnouts et al. 2002); the *JK* images from GOODS (Giavalisco et al. 2004); and the *JK* images from the EIS Deep Infrared Survey at eso.org/science/eis/surveys/strategy_EIS-deep_infrared_survey.html. We also added the *Chandra* images from

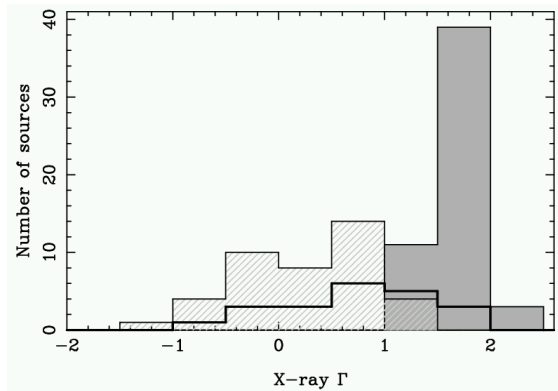


FIG. 1.— Distribution of X-ray photon index Γ (defined as $f_\nu \propto \nu^{1-\Gamma}$). Plotted are the optically-faint CSS AGN (thick line); X-ray-selected Type 1 AGN (shaded region); and X-ray-selected Type 2 AGN (cross-hatched region). Classifications are from Szokoly et al. (2004). Photon index values are from Alexander et al. (2003); we omit sources where Γ is undetermined or is uncertain by more than ± 0.5 .

astro.psu.edu/users/niel/hdf/hdf-chandra.html (Alexander et al. 2003).

For each source, any object detected in the K band within $2''$ of the X-ray position was selected for photometry in all available bands. The source selections were reviewed visually, and when necessary, were modified so that the same source was photometered in each band. The result is closely-sampled, deep photometry from 0.4 to $8 \mu\text{m}$, with additional coverage at $24 \mu\text{m}$.

We now discuss the few sources that have multiple K-band components within $2''$, where extra care was needed to obtain accurate photometry:

AID 100: There are four K-band sources (or components) within $3''$ of the X-ray position, with offsets of $0.1, 1.3, 2.9$, and $2.9''$. These same components are also present in the ACS z-band image. We quote photometry for the closest ($0.1''$ offset) source.

AID 218: The K-band counterpart is clearly the source located only $0.3''$ from the X-ray coordinates. However, a second source (located $2.1''$ from the X-ray source, and $1.5''$ from the K-band counterpart) contaminates the measured IRAC fluxes in channels 2–4. Therefore, we plot these fluxes as upper limits in figure 2.

AID 241: There are two K-band components, one located $0.4''$ away, and a fainter source $1.6''$ from the X-ray position. We photometer the closer source.

AID 245: There are two K-band components, located $0.4''$ and $1.9''$ from the X-ray position. The measured IRAC fluxes are contaminated by contribution from the farther component.

AID 281: There is a K and ACS source $0.3''$ from the X-ray coordinates; it appears to be extended (or double) out to $0.7''$ from the X-ray source. We photometer only the closer component of the extended source.

4. PROPERTIES OF THE COMPLETE SED SAMPLE

4.1. Spectral Properties

Figure 1 shows the distribution of X-ray photon index Γ (defined as $f_\nu \propto \nu^{1-\Gamma}$) for the CSS. Unobscured AGN generally have $\Gamma \approx 2$ (and are thus flat in νf_ν), whereas obscured AGN generally have $\Gamma \lesssim 1$ (and thus

⁴ The rest have fluxes in agreement within a factor of two.

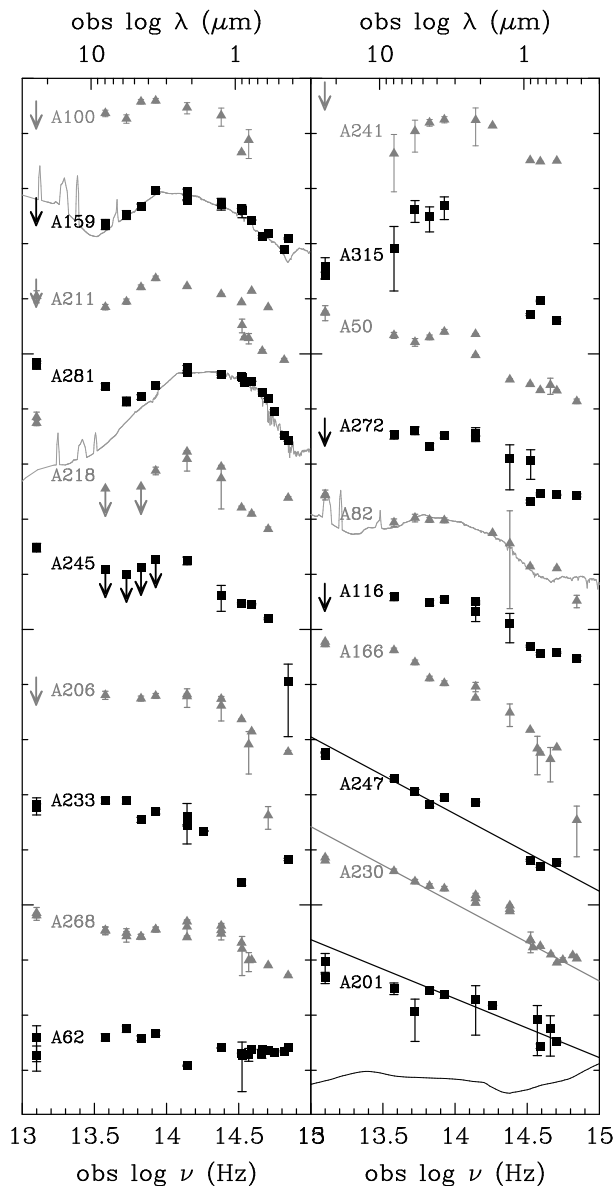


FIG. 2.— The sample of complete SEDs. Sources with strong stellar features are plotted first, progressing to weaker stellar features and finally to sources with power-law SEDs. Wavelengths and frequencies are as observed. For illustration, we overplot three templates from Devriendt et al. (1999): M82 with an additional $E(B-V)=0.2$ of reddening (plotted with source AID 159); early-type galaxy Virgo 1003 (plotted with AID 281); and rapidly star-forming galaxy IRAS 05189-2524 from Devriendt et al. (1999) (plotted with AID 82). We also plot the median Type 1 QSO spectrum of Elvis et al. (1994) (bottom right) in order to illustrate how much redder are the optically-faint AGN.

νf_ν rises with increasing frequency). The optically-faint Γ distribution appears to be intermediate in obscuration, with a significant number of obscured AGN.

The 0.4–24 μm spectral energy distributions of the CSS are plotted in figure 2. Optical through 24 μm photometry is reported in table 1; X-ray photometry is reported in table 2. All but 3–4 of the SEDs show strong stellar features—either breaks or the characteristic broad stellar hump peaking near 1.6 μm rest-frame. The remaining sources show a red, power-law continuum, with a spectral break between 8 and 24 μm .

4.2. Redshift Techniques and Previously-Estimated Redshifts

There are three published spectroscopic redshifts for CSS sources, measured by Szokoly et al. (2004) and listed in our table 1. Of these, AID 230 and 245 have redshifts of $z = 1.603$ and $z = 3.064$, respectively. Also, for AID 241 there is a published redshift of $z = 0.679$ for an optical counterpart 1.6'' from the Alexander et al. (2003) position (which is source number 201b in Szokoly et al. 2004). However, we feel that this is not the most likely counterpart to the X-ray source, since there is a closer, fainter source: Szokoly source 201a, located just 0.6'' from the Alexander et al. (2003) position. This closer source lacks a spectroscopic redshift.

Since only a few spectroscopic redshifts are available for the sample, one must turn to photometric techniques. Two groups, Zheng et al. (2004) and COMBO-17 (Wolf et al. 2004), have estimated photometric redshifts for some of the CSS sources. The former group used 10 photometric bands from 0.3 to 2.1 μm ; the latter group used 17 passbands from 0.35 to 0.93 μm . The redshift estimates from these two groups, as applicable to the CSS, are compiled in table 1.

Adding IRAC fluxes to photometric redshift methods should dramatically improve the results, since IRAC samples the peak and red side of the stellar emission out to high redshift. Several groups are currently searching for the best way to do exactly that—the question is not trivial, partly because of the lack of good templates over this wide redshift range. One solution, adopted by Pérez-González et al. (2005), is to use empirical templates compiled from sources in deep fields that have spectroscopic redshifts, and then use those templates to fit photometric redshifts to other faint sources. Their photo- z technique is described in detail in the appendix to that paper.

Unfortunately, for galaxies that host AGN, template-fitting of any sort (whether the high-resolution templates of standard photo- z techniques, or the low-resolution templates used by (Pérez-González et al. 2005)) can be difficult and potentially unreliable. First of all, each source has a differing contribution of host galaxy and AGN light. Secondly, some of the high-redshift, red AGN have SED shapes that are quite different from the templates, which are based on lower-redshift, bluer samples.

Clearly, caution is warranted when resorting to photometric redshifts, since the techniques are unproven when applied to sources as extreme as the optically-faint AGN. Different techniques of redshift determination should be tested against each other for consistency, and the widest possible range of templates should be used.

4.3. New Photometric Redshift Estimations

To estimate redshifts from our 0.4–8 μm data, we adopt a different, more conservative approach than simply adopting the results of a best-template fitting program. Our goal is not to find the best or most likely redshift, but rather to constrain the redshift range of each source with high confidence.

In our technique, we manually compared the photometry of each source to a range of SED templates from Devriendt et al. (1999), namely the early-type galaxy Virgo 1003, spiral galaxies including Virgo 1987, the star-

burst galaxy M82, and the ultraluminous infrared galaxy IRAS 05189-2524. We chose these templates to sample a wide range of star formation rate.

In a few cases, we needed to add extra reddening (a few tenths of a magnitude in $E(B-V)$) to the Devriendt et al. (1999) templates to match the optical fluxes, since these sources are much redder than the Devriendt et al. (1999) galaxies. (For example, see AID 281 in figure 2). We also add varying amounts of dust to make sure our redshift results are not highly dependent on the chosen extinction.⁵

For each source, we compare these templates to the photometry, and find the redshift range for which *any* template provides a good match to the photometry. For example, a source might be fit by the M82 template at $1 < z < 1.3$, as well as by the M82 template with added extinction at $0.8 < z < 1.1$. In this case, we would quote the range $0.8 < z < 1.3$.

Our resulting redshift ranges are tabulated in table 1.

Our redshift ranges agree reasonably well with the other techniques. In 10 out of 13 cases, our redshifts agree with those of Zheng et al. (2004). We quote redshifts for four sources where Zheng et al. (2004) did not, and they quote redshifts for two power-law objects where we do not. COMBO-17 lists three redshifts for CSS sources; we can estimate redshifts for two, and agree in one case. Three CSS sources have spectroscopic redshifts; our photo-zs agree in two cases (AID 166 and 230), and strongly disagree in one case (AID 245, with $z_{spec} = 3.064$, for which we securely find $z=1.1-1.4$).

Thus, 12 CSS sources (57%) have redshifts confirmed by two different techniques (COMBO-17 and our method, or Zheng et al. (2004) and our method). Also, five additional CSS sources have single-source redshift estimates at high confidence (four from our technique, and one from Szokoly et al. (2004).) Thus, 17/20 CSS sources (85%) have useful redshift information.

We can also test the agreement between our redshift estimates and those found using the empirical template technique of Pérez-González et al. (2005). For 11 of the 17 sources with useful redshift information, the Pérez-González et al. (2005) photo-z falls within the quoted redshift range. This is fairly good agreement, considering that the empirical template technique has not been optimized to deal with AGN SEDs.

One notable problem with the photometric redshifts is the case of AID 245. It's spectroscopic redshift of $z=3.065$ (Szokoly et al. 2004), based on two narrow emission lines, appears to be solid. However, we have estimated its redshift as 1.0–1.3. The photometry is well-measured, so why is the photometric method in such disagreement with the spectroscopic redshift?

We inferred a redshift of $z \sim 1$ for AID 245 based on the apparent stellar hump from $\lambda_{obs} = 1.6-6 \mu\text{m}$, with peak at $\sim 3 \mu\text{m}$. Such a spectral shape is not consistent with any stellar template at $z \sim 3$ (which should peak in emission at $\lambda_{obs} \sim 6.5 \mu\text{m}$). Clearly, the problem is not with the template-fitting, but with the photometry.

Close examination of the images indicates that the

IRAC photometry of AID 245 is contaminated by a neighboring source. Thus, the photometry is probably a composite of two sources, which together simulate a stellar hump at $z \sim 1$. This could explain why the hump appears narrower (and rises more quickly from J to K-band) than stellar templates.

Thus, it appears that the redshift discrepancy for AID 245 results from a perverse case of source blending, in that the composite SED looks stellar (but at a fictitious redshift) rather than obviously composite. In section § 3, we looked for evidence of other blending problems, and found that cases like AID 245 are rare in the CSS sample.

4.4. The Redshift Distribution of the Optically-Faint CSS AGN

We now consider the redshifts of the 17/20 CSS sources with useful redshift information. When a spectroscopic redshift has been published, we use it; otherwise, we use the redshift ranges found using our technique in §4.3.

Almost all (14/17) of the CSS AGN lie at $z > 1$, and at least 25% lie at $z > 2$. By contrast, of the 99 reliable⁶ spectroscopic redshifts available for X-ray-selected AGN in CDFS (Szokoly et al. 2004), only 42% lie at $z > 1$; only 17% lie at $z > 2$. Thus, the optically-faint X-ray sources lie at higher redshift than other X-ray-selected AGN, although their redshifts are typical of the optical QSO population.

Since the redshift distribution of optically-bright AGN in CDFS is strongly influenced by large-scale structure (two redshift spikes at $z = 0.674$ and 0.734), we now compare with several other fields. Gilli (2003) has compiled the redshift distribution of X-ray-selected sources with $f_{2-10\text{keV}} > 5 \times 10^{-15} \text{ erg s}^{-1} \text{ cm}^{-2}$ in CDFS, CDFN, Lockman Hole, Lynx field, and SSA13. After excluding large scale structures from CDFN and CDFS, 49% of the sources lie at $z > 1$, and 14% lie at $z > 2$. This distribution, too, lacks high-redshift objects compared with our results for the optically-faint AGN.

4.5. The Luminosity Function of Optically-Faint AGN

We now compute the rest-frame 2–8 keV luminosity function of optically-faint AGN. We use the standard V_{max} method (Schmidt 1968; Huchra & Sargent 1973), and do not correct for incompleteness.⁷ We assume $\Omega_m = 0.27$, $\Omega_\Lambda = 0.73$, $H_0 = 72$. Because the X-ray sensitivity varies strongly over the field, we calculate V_{max} for each source by summing the volume contribution from each *Chandra* pixel in the GOODS ACS field. The 5σ limiting flux in each pixel was calculated by the method of Muno et al. (2003), using the CDFS exposure map (Alexander et al. 2003) and an analytic approximation of the *Chandra* PSF⁸.

Figure 3 plots the resulting LF, based on the redshift constraints given in table 1 (using the spectroscopic redshift if available, and otherwise our redshift range found in §4.3.) Within the GOODS ACS field, there are 27 optically-faint sources with high-confidence hard-band detections (detected by both Alexander et al. 2003 and Giacconi et al. 2002); of these, we found redshift

⁵ We do not bother to add this absorbed UV and optical energy back to the templates as re-emitted infrared light, since it would only contaminate the longest, non-stellar wavelengths which are not important in stellar feature fitting.

⁶ “Reliable” in this context means a quality flag $Q \geq 2$.

⁷ since we do not know the intrinsic V/V_{max} distribution.

⁸ <http://cxc.harvard.edu/chandra-users/0195.html>

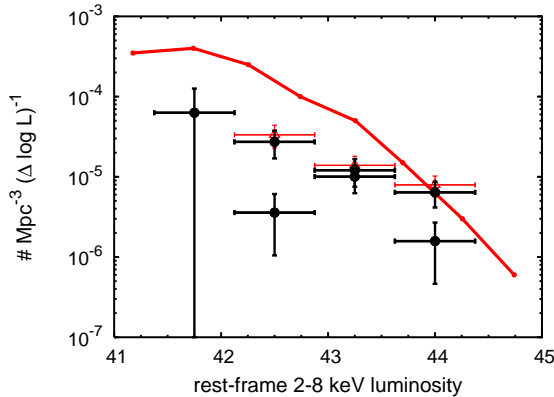


FIG. 3.— The rest-frame 2–8 keV AGN luminosity function. Filled circles show the optically-faint AGN LF, computed using the 17 CSS AGN with constrained redshifts. We compute this LF twice, once using the lowest permitted redshift for each source, and again using the highest redshift. The LF has been corrected for known AGN lacking redshifts (see § 4.5); we do not otherwise correct for incompleteness. For comparison, we plot the $0.1 < z < 1$ LF (red solid line) for AGN with spectroscopic redshifts (Steffen et al. 2003). We also compute the LF for those $1 < z < 4$ AGN in the GOODS field with Szokoly et al. (2004) redshifts (red triangles).

information for 17. Therefore, we have multiplied the optically-faint AGN LF found for the 17 sources by 27/17 (which assumes the redshift distributions are similar.)

For comparison, we plot the spectroscopically-determined rest-frame 2–8 keV LF for X-ray-selected AGN from $0.1 < z < 1.0$ (Steffen et al. 2003). Two general conclusions are apparent. First, the optically-faint AGN are not terribly luminous—most have $\log L_x \sim 42.5\text{--}44 \text{ erg s}^{-1}$. Thus, we sample lower luminosities than the optically-faint QSOs discovered in shallow, wide-field surveys, (Fiore et al. 2003; Mignoli et al. 2004; Brusa et al. 2004) as expected given the survey sensitivities. Second, the number density of the optically-faint AGN in CDFS is comparable to that of $1 < z < 4$ AGN that have been identified by optical spectroscopy. Therefore, optically-faint AGN boost the high-redshift tail of the X-ray-selected AGN redshift distribution, but only by a factor of ~ 2 .

Thus, we find that the optically-faint sources have moderate redshifts ($1 < z < 3$) and Seyfert luminosities ($\log L_{2-8\text{keV}} < 44 \text{ erg s}^{-1}$), rather than higher redshifts and QSO luminosities. As such, they are not expected to contribute strongly to the X-ray background, as compared to $z < 1$ Seyferts and $z > 2$ QSOs (see for example figures 16 and 17 of Ueda et al. (2003)). Several techniques are presently being tested to identify additional high-obscuration AGN (for example, see Alonso-Hererro et al. (2005) and Donley et al. (2005)). When results from such studies are available, it will be valuable to determine the overlap between selection methods, calculate the discovered sources' contribution to the X-ray background (as well as the contribution from the optically-faint AGN), and re-evaluate what fraction of the obscured AGN have been identified.

5. OTHER OPTICALLY-FAINT SOURCES

Some sources, especially at high redshift, may be too faint to be identified by our f_X/f_R flux criterion. Further, absorption from the Lyman α forest will suppress the R-band flux for $z \gtrsim 4$.

Therefore, we examine the most extreme optically faint cases: X-ray detections that are undetected even in extremely deep $z' > 28$ imaging with HST. Koekemoer et al. (2004) have identified seven such sources in the CDFS/GOODS field, and suggested they may lie at $z > 6$ or be very dusty. To test the nature of these AGN, we have combined the *Spitzer* bands with the GOODS photometry (Koekemoer et al. (2004)). We find several source categories: 1.) Source K4 is an X-ray detection, but an otherwise blank field—lacking an optical, near-infrared, or *Spitzer* counterpart; 2.) Sources K1 and K6 have power-law SEDs; and 3.) Sources K2, K3, and K7 have stellar-featured SEDs, with nominal photometric redshifts of $z \sim 3$, $z \sim 2$, and $2 < z < 6$ respectively. Source K5 is intermediate between these last two categories.

A number of optically-faint sources outside the CSS have steep power-law SEDs: AID 4, 42, 45, 64, 79, 92, and 283. They may be related to the optically-faint, power-law members of the flat spectrum 1 Jy (at 5 GHz) sample (Stickel et al. (1996)). The faint 1 Jy power-law sources have spectral indices $\alpha \geq -2.5$ (with α defined as $f_\nu \propto \nu^\alpha$). The spectral indices of our objects are listed in table 1; they are generally in agreement with the limit derived by Stickel et al. (1996) for the radio sample. The steep power law sources comprise only about 2% of the flat spectrum 1 Jy sample; their incidence in the CDFS appears to be as high or higher.

6. CONCLUSIONS

We report reliable (e.g. confirmed by independent methods) photometric redshifts for a representative sample of optically-faint X-ray sources in the CDFS. We find that they have higher redshifts ($z > 1$) than most X-ray-selected AGN, but only $\sim 30\%$ lie at $z > 2$. Thus, they populate the redshifts where optical QSOs are most numerous. Their $0.4\text{--}24 \mu\text{m}$ SEDs are intrinsically redder than typical AGN, and notably lack bright blue continua. Their X-ray spectra indicate significant absorption. Their X-ray luminosities are modest ($\log L_x \sim 42.5\text{--}44 \text{ erg s}^{-1}$), and they boost the high-redshift tail of the X-ray-selected AGN distribution by a factor of 2.

This work is based in part on observations made with *Spitzer*, which is operated by the Jet Propulsion Laboratory, California Institute of Technology under NASA contract 1407. Support for this work was provided by NASA through Contract Number 960785 issued by JPL/Caltech.

REFERENCES

Alexander, D. M., et al. 2003, AJ, 126, 539

Alexander, D. M., Brandt, W. N., Hornschemeier, A. E., Garmire, G. P., Schneider, D. P., Bauer, F. E., & Griffiths, R. E. 2001, AJ, 122, 2156

- Alonso-Hererro, A. et al. 2005, in preparation.
- Arnouts, S., Vandame, B., Benoist, C., Groenewegen, M. A., da Costa, L., Schirmer, M., Mignani, R. P., & Slijkhuis, R. 2002, VizieR Online Data Catalog, 337, 90740
- Barger, A. J., Cowie, L. L., Bautz, M. W., Brandt, W. N., Garmire, G. P., Hornschemeier, A. E., Ivison, R. J., & Owen, F. N. 2001, *AJ*, 122, 2177
- Barger, A. J., et al. 2003, *AJ*, 126, 632
- Bregman, J. N., Glassgold, A. E., Huggins, P. J., & Kinney, A. L. 1985, *ApJ*, 291, 505
- Brusa, M., et al. 2004, *A&A*, submitted, astro-ph/0409257
- Comastri, A., et al. 2002, astro-ph/0211306
- Cowie, L. L., Barger, A. J., Brandt, W. N., & Garmire, G. P. 2003, *ApJ*, 584, L57
- Devriendt, J., Guiderdoni B. & Sadat, R. 1999, *A&A*, 350, 381
- Donley, J. L. et al. 2005, in preparation
- Elvis, M. et al. 1994, *ApJS*, 95, 1
- Fazio, G. G., et al. 2004, *ApJS*, 154, 10
- Fiore, F., et al. 2003, *A&A*, 409, 79
- LeFevre et al. 2004, *A&A*, submitted
- Giacconi, R., et al. 2002, *ApJS*, 139, 369
- Giavalisco, M., et al. 2004, *ApJ*, 600, L93
- Gilli, R. 2003, to appear in *New X-ray Results from Clusters of Galaxies and Black Holes*, ed. C. Done et al. (astro-ph/0303115)
- Gilli, R., Risaliti, G., & Salvati, M. 1999, *A&A*, 347, 424
- Gilli, R., Salvati, M., & Hasinger, G. 2001, *A&A*, 366, 407
- Gordon, K., et al., *PASP*, submitted
- Huchra, J., & Sargent, W. L. 1973, *ApJ*, 186, 433
- Koekemoer, A. M., et al. 2004, *ApJ*, 600, L123
- Maccacaro, T., Gioia, I. M., Wolter, A., Zamorani, G., & Stocke, J. T. 1988, *ApJ*, 326, 680
- Marzke et al. 1999, in *PASP Conf. Ser.* 191: Photometric Redshifts and Detection of High Redshift Galaxies, 148
- Mignoli, M., et al. 2004, *A&A*, 418, 827
- Moretti, A., Campana, S., Lazzati, D., & Tagliaferri, G. 2003, *ApJ*, 588, 696
- Muno, M. P., et al. 2003, *ApJ*, 589, 225
- Pérez-González, P. G., et al. 2005, in preparation
- Rieke, G. H., et al. 2004, *ApJ*, 154, 25
- Rigby, J. R., et al. 2004, *ApJS*, 154, 160
- Schmidt, M. 1968, *ApJ*, 151, 393
- Steffen, A. T., Barger, A. J., Cowie, L. L., Mushotzky, R. F., & Yang, Y. 2003, *ApJ*, 596, L23
- Stickel, M., Rieke, G. H., Kühr, H., & Rieke, M. J. 1996, *ApJ*, 468, 556
- Szokoly, G. P., et al. 2004, *ApJS*, 155, 271 (catalog at <http://www.mpe.mpg.de/CDFS>)
- Ueda, Y., Akiyama, M., Ohta, K., & Miyaji, T. 2003, *ApJ*, 598, 886
- Werner, M. W., et al. 2004, *ApJS*, 154, 1
- Wolf, C., et al. 2004, *A&A*, 421, 913
- Yan, H., Windhorst, R. A., Röttgering, H. J., Odewahn, S. C., Chapman, S. C., & Keel, W. C. 2003, *ApJ*, 585, 67
- Zheng, W. et al. 2004, *ApJS*, 155, 73

TABLE 1
MULTI-BAND PHOTOMETRY AND REDSHIFTS FOR THE OPTICALLY–FAINT AGN SAMPLE.

AID/XID	optical	Ks	3.6 μ m	4.5 μ m	5.7 μ m	8.0 μ m	24 μ m	α	Lit. redshift	Our redshift
50/227	R= 0.24 ± 0.08	4.7 ± 2	12 ± 1	12 ± 1	12.4 ± 2	23.0 ± 3	180 ± 55	-2.3	$2.18 (1.78-2.54)^1$	2.8–3.5
62/64	R= 0.76 ± 0.07	1.39 ± 0.03	8.9 ± 0.9	9 ± 1	17 ± 2	17 ± 2.4	49 ± 30	-0.88	1.27 ± 0.2^2	...
82/58	z= 0.26 ± 0.01	...	7.2 ± 0.7	9 ± 1	1.3 ± 2	15 ± 2	141 ± 28	-2.0	$0.92 (0.58-1.22)^1$	1.8–3.8
100/82	i= 0.65 ± 0.3	6.7 ± 3	15 ± 1.4	18 ± 1.7	11 ± 2	20 ± 3.0	< 98		$1.89 (1.69-2.05)^1$	1.1–1.8
116/205	i= 0.15 ± 0.01	3.1 ± 0.6	6.6 ± 0.7	7.3 ± 0.8	...	16 ± 2	< 86	-2.3	$1.56 (1.31-2.3)^1$	1.3–1.5
159/48	R= 0.46 ± 0.03	8.5 ± 1.5	17 ± 2	11.6 ± 1	10.1 ± 2	9.6 ± 2	< 86		$1.26 (1.03-1.49)^1$	0.7–1.1
166/45	R= 0.11 ± 0.07	6.0 ± 1.4	14 ± 1	21.8 ± 2	53.9 ± 5	125 ± 12	480 ± 45	-2.6	$2.29 (2.14-2.60)^3$	1.0–2.5
201/515	R= 0.13 ± 0.09	1.4 ± 1.1	2.8 ± 0.4	4.2 ± 0.5	2.2 ± 1.5	8.2 ± 2	75 ± 30	-2.1	$2.19 (2.15-2.45)^1$	1.3–4.8
206/265	i= 0.29 ± 0.01	3.6 ± 0.2	5.9 ± 0.6	6.7 ± 0.7	...	14 ± 2	< 86		$1.16 (1.02-1.32)^1$	1.0–1.4
211/35	R= 0.39 ± 0.02	19 ± 0.4	44 ± 4	39 ± 4	27 ± 3	30 ± 3	140 ± 35		1.14 ± 0.14^2	0.9–1.4
218/148	i= 0.064 ± 0.005	2.1 ± 0.3	1.8 ± 0.3	< 1.2	...	< 1.9	112 ± 27		$1.74 (1.50-2.02)^1$...
230/31	R= 0.55 ± 0.03	18.8 ± 3	47 ± 4	$66. \pm 6$	100 ± 9	217 ± 20	1008 ± 62		$1.603^4; 1.1 \pm 0.1^2$	1.5–2.0
233/79	z= 0.097 ± 0.01	3.1 ± 0.6	7.4 ± 0.7	6.7 ± 0.7	19 ± 2	26 ± 3	65 ± 22	-1.8	$1.91 (1.77-1.97)^1$	1.0–2.5
241/201	i= 0.098 ± 0.007	1.6 ± 1	2.7 ± 0.3	3.0 ± 0.4	2.6 ± 1.5	1.4 ± 1.4	< 86	-0.90	$0.679^{4a}; 0.14, 1.0^2$	1.5–2.2
245/27	i= 0.47 ± 0.02	8.0 ± 1.3	< 14	< 12.6	< 12	< 20	155 ± 28	-2.0	3.064^4	1.0–1.4
247/25	i= 0.21 ± 0.01	8.4 ± 0.1	16.5 ± 2	16 ± 1.5	34 ± 4	82 ± 8	660 ± 50	-2.4	$2.26 (1.89-2.58)^1$	1.7–4.7
268/147	i= 0.41 ± 0.01	4.4 ± 1	6.8 ± 0.7	6.3 ± 0.7	8.1 ± 2	15 ± 2	90 ± 23	-2.0	$0.99 (0.79-1.21)^1$	0.8–1.1
272/146	i= 0.12 ± 0.01	3.9 ± 0.2	6.2 ± 0.6	5.0 ± 0.6	12 ± 2	14 ± 2	< 86	-2.5	$2.67 (2.47-2.85)^1$	2.4–3.4
281/159	R= 1.7 ± 0.08	14.6 ± 1.5	12 ± 1	9.9 ± 1	11 ± 2	27 ± 3	200 ± 36		$3.30 (3.04-3.62)^1$	0.2–0.6
315/506	i= 1.0 ± 0.1	...	260 ± 115	210 ± 100	360 ± 150	100 ± 100	140 ± 60	-2.9	$3.69 (3.12-4.19)^1$...

NOTE. — Column 1: AID/XID are the source identification numbers in the Alexander et al. (2003) and Giacconi et al. (2002) catalogs, respectively. Column 2 is optical flux density: we quote R-band when available, then i, then z. Columns 2–8: optical, Ks, IRAC, and MIPS flux densities are all listed in μ Jy. Column 9: the 0.4–8 μ m spectral index α is defined in the text. Column 10: “Lit. Redshift” is the source redshift found in the literature. Column 11: “Our Redshift” is the redshift found using our techniques, as described in the text. REFERENCES— [1] Photometric redshift using BPZ and HyperZ, from Zheng et al. (2004); [2] Photometric redshift from Combo-17 (Wolf et al. 2004); [3] Redshift from single-line spectrum (Szokoly et al. 2004) and HyperZ, from Zheng et al. (2004); [4] Spectroscopic redshift from Szokoly et al. (2004).

^aReshift is for optical source 201b listed by Szokoly et al. (2004). We suspect the true optical counterpart is Szokoly 201a, which lacks a spec. redshift.

TABLE 2
X-RAY PHOTOMETRY FOR THE OPTICALLY–FAINT AGN SAMPLE.

AID/XID	offset	0.5–2 keV flux	2–8 keV flux	X-ray Γ
50/227	0.4	1.2 ± 0.4	36.2 ± 5.2	$-0.43^{+0.31}_{-0.32}$
62/64	0.2	21.7 ± 1.2	55.2 ± 4.7	1.36 ± 0.09
82/58	0.2	7.1 ± 0.7	19.6 ± 3.1	$1.30^{+0.18}_{-0.16}$
100/82	0.4	2.4 ± 0.4	15.1 ± 2.8	$0.71^{+0.24}_{-0.22}$
116/205	0.3	1.5 ± 0.5	14.4 ± 4.1	$0.41^{+0.41}_{-0.37}$
159/48	0.9	9.1 ± 0.9	48.6 ± 5.4	0.83 ± 0.13
166/45	0.4	10.9 ± 0.9	49.4 ± 4.9	$0.94^{+0.12}_{-0.11}$
201/515	0.3	0.9 ± 0.3	15.1 ± 3.0	$0.02^{+0.33}_{-0.31}$
206/265	0.5	2.2 ± 0.5	40.8 ± 5.8	-0.08 ± 0.25
211/35	0.9	40.8 ± 6.4	142.0 ± 35	$1.13^{+0.28}_{-0.24}$
218/148	0.5	3.9 ± 0.5	28.5 ± 3.8	$0.61^{+0.18}_{-0.17}$
230/31	0.3	59.7 ± 1.9	87.8 ± 5.2	1.75 ± 0.06
233/79	0.2	8.8 ± 0.9	15.5 ± 2.8	$1.62^{+0.19}_{-0.18}$
241/201	0.3	4.6 ± 0.6	21.4 ± 3.4	$0.93^{+0.19}_{-0.18}$
245/27	0.3	7.5 ± 0.7	70.6 ± 5.6	0.42 ± 0.11
247/25	1.0	5.4 ± 0.7	93.4 ± 7.9	-0.02 ± 0.14
268/147	0.1	1.9 ± 0.4	72.6 ± 7.0	-0.61 ± 0.22
272/146	1.1	4.6 ± 0.6	25.5 ± 4.0	$0.81^{+0.19}_{-0.18}$
281/159	0.7	24.0 ± 1.3	75.3 ± 5.7	1.21 ± 0.08
315/506	0.7	6.9 ± 0.9	9.3 ± 3.7	$1.81^{+0.45}_{-0.33}$

NOTE. — Column 1: AID/XID are the source identification numbers in the Alexander et al. (2003) and Giacconi et al. (2002) catalogs, respectively. Column 2: “Offset” is the offset (in $''$) between the Alexander et al. (2003) and Giacconi et al. (2002) X-ray coordinates. Column 3–4: X-ray fluxes are quoted from Alexander et al. (2003), and have units of 10^{-16} erg s $^{-1}$ cm $^{-2}$. Column 5: The X-ray photon index Γ is defined in the text.